ACS APPLIED MATERIALS & INTERFACES

Research Article

www.acsami.org

# Direct-Write Fabrication of 4D Active Shape-Changing Structures Based on a Shape Memory Polymer and Its Nanocomposite

Hongqiu Wei,[†] Qiwei Zhang,[†] Yongtao Yao,[†] Liwu Liu,[‡] Yanju Liu,[‡] and Jinsong Leng*[,†]

[†]Center for Composite Materials and Structures and [‡]Department of Astronautical Science and Mechanics, Harbin Institute of Technology (HIT), Harbin 150080, People's Republic of China

Supporting Information

**ABSTRACT:** Four-dimensional (4D) active shape-changing structures based on shape memory polymers (SMPs) and shape memory nanocomposites (SMNCs) are able to be controlled in both space and time and have attracted increasing attention worldwide. However, conventional processing approaches have restricted the design space of such smart structures. Herein, 4D active shape-changing architectures in custom-defined geometries exhibiting thermally and remotely actuated behaviors are achieved by direct-write printing of ultraviolet (UV) cross-linking poly(lactic acid)-based inks. The results reveal that, by the introduction of a UV cross-linking agent, the printed objects present excellent shape memory behavior, which enables three-dimensional (3D)−one-dimensional (1D)−3D, 3D−two-dimensional (2D)−3D, and 3D−3D−3D configuration transformations. More importantly, the addition of iron oxide successfully integrates 4D shape-changing objects with fast remotely actuated and magnetically guidable properties. This research realizes the printing of both SMPs and SMNCs, which present an effective strategy to design 4D active shape-changing architectures with multifunctional properties. This paves the way for the further development of 4D printing, soft robotics, flexible electronics, minimally invasive medicine, etc.

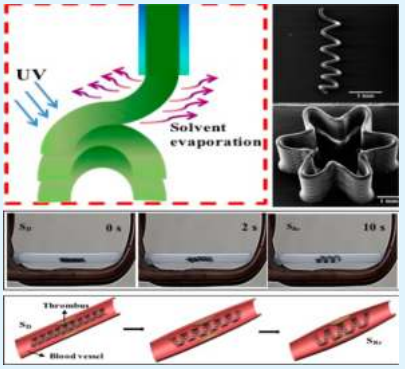


**KEYWORDS:** *direct-write fabrication, 4D shape-changing structures, shape memory polymer, shape memory nanocomposite, remotely actuated behavior*



## INTRODUCTION

Shape memory polymers (SMPs), a kind of stimulus-responsive material, are capable of recovering their initial shape in the presence of an external stimulus after going through a shape deformation.[1−4] On the basis of this unique shape memory effect, SMP-based materials could be used to construct architectures possessing active shape-changing behaviors.[5,6] Because of their potential applications in areas ranging from aerospace to human body, such types of smart structures have enjoyed extensive academic and industrial interest in the past decades.[7−13] However, the investigation and application of active shape-changing structures fabricated by SMP-based materials are far from fully exploited.[14] One of the most important reasons is that most SMP-based materials are difficult to fabricate into active shape-changing architectures with user-defined geometries and sizes because of the limitations of conventional processing technologies.[15] This significantly restricts their development in various fields like soft robotics, flexible electronics, biomedical devices, and four-dimensional (4D) printing.[16−18]

Additive manufacturing, or 3D printing, which is an emerging way to process materials into complex structures,[19−24] shows promise in its application to a diverse group of research fields ranging from medical industry to architectural design.[24−28] With the increasing maturity and popularity of 3D printing, several strategies have been carried out to fabricate SMP-based 4D active shape-changing architectures.[15,29−31] Qi et al. proposed that SMPs are excellent materials to realize 4D printing based on their time dependence of shapes upon exposure to an external stimulus.[31] By 3D printing digital SMPs as hinges, they successfully designed sequential self-folding structures that could be applied to self-assembling robots, medical devices, etc.[30] Cohn et al. developed shape memory oligomer melts that could be printed by a stereolithography 3D digital light-processing printer. They further demonstrated the feasibility of using such SMP-based 4D active shape-changing architectures for flexible devices and circuits.[15] The studies above open the way for the fabrication of a SMP-based 4D active shape-changing configuration, while the actuated method of these architectures focuses on direct heating. Such a traditional external stimulus is difficult to manipulate in most practical applications because all structures including the surrounding environment have to be heated.[2,32] The utilization of shape memory nanocomposites (SMNCs) with magnetic iron oxide ($Fe_3O_4$) nanoparticles is advantageous because the $Fe_3O_4$ nanoparticles can be remotely heated by alternating magnetic fields.[33−37] It may be an effective strategy to realize the self-heating of SMP-based 4D active shape-changing

**Received:** October 9, 2016
**Accepted:** December 12, 2016
**Published:** December 20, 2016




DOI: 10.1021/acsami.6b12824
ACS Appl. Mater. Interfaces 2017, 9, 876−883

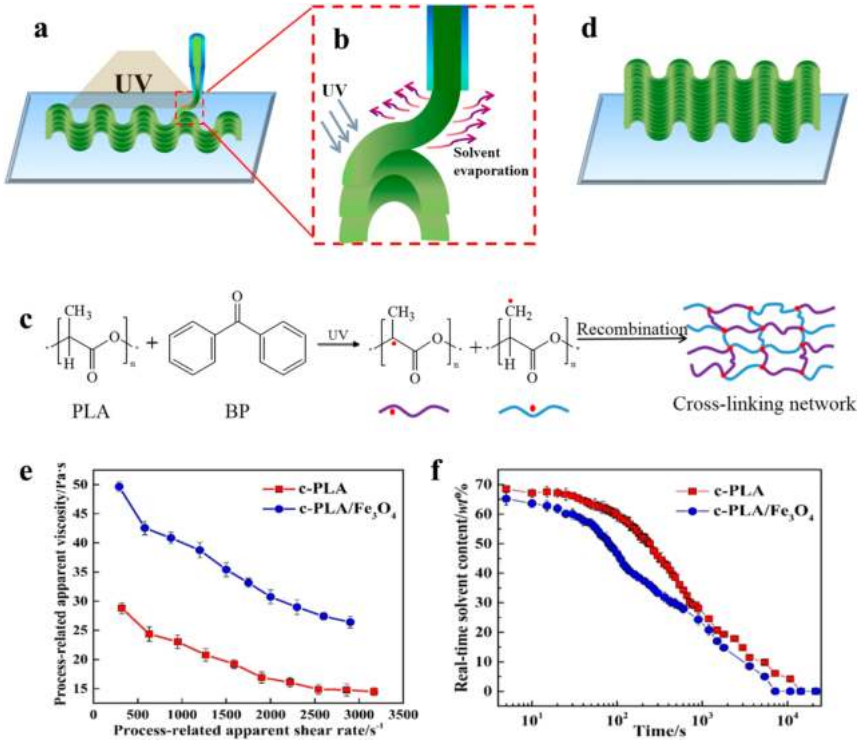


**Figure 1.** Schematic illustration of the DW printing of 4D active shape-changing architecture and the properties of inks: (a) extrusion of UV cross-linked PLA-based ink from a micronozzle under a suitable applied pressure; (b) fast solvent evaporation after extrusion; (c) UV cross-linking reaction triggered during the depositing process; (d) example of a printed 3D waviness-like configuration with potential shape-changing behavior; (e) process-related apparent viscosity versus process-related apparent shear rate; (f) real-time solvent content as a function of time.

architectures. However, the printing of SMNCs remains difficult to achieve because most 3D printers are designed to print only pure polymers with limited choices.

Direct-write (DW) printing techniques, reported by Lewis et al. and Therriault et al.,[38−44] can be designed to match various classes of materials such as polyelectrolytes,[44] ultraviolet (UV)-curable polymers,[42] colloidal suspensions,[39] polymeric solutions,[40] etc. By combining with such an assembly, herein, we demonstrated the possibility of building 4D active shape-changing architectures by both polymer- and nanocomposite-based inks. Poly(lactic acid) (PLA) was chosen as the principle material because of its widespread investigation in the shape memory area.[36,45−47] To make it 3D printable, PLA was dissolved in dichloromethane (DCM). Benzophenone (BP) and $Fe_3O_4$ were further introduced to achieve excellent shape memory and remotely actuated characteristics, respectively. We first investigated the rheological properties of the inks and the evaporation performance of DCM during the printing process. In what follows, the macroscopic properties of the printed objects were analyzed in detail. We successfully printed several 4D structures by both polymer- and nanocomposite-based inks. Their thermally and remotely actuated active shape-changing performances were disscussed. We further explored the potential application of such smart structures in biomedical areas.

## RESULTS AND DISCUSSION

The key components of the DW assembly include a microdepositing robot controlled by computer software, a dispensing apparatus, and two UV light-emitting diodes (LEDs). Parts a−d of Figure 1 schematically described the DW printing process. The prepared ink was put into a syringe with a micronozzle and fixed onto the robot head. The ink was extruded through the nozzle by imposing a suitable pressure (Figure 1a). Once the ink was forced out, the fast evaporation of the solvent and the high solid concentration enabled the ink to complete a liquid−solid transition rapidly, which was crucial for the fabrication of filaments (Figure 1b). UV LEDs were utilized in the printing process to trigger the cross-linking reaction[48,49] (Figure 1c) that was indispensable for excellent shape memory behavior. User-defined structures could be constructed by adjusting the pressure, moving the velocity and direction of the robot appropriately (Figure 1d).

To construct 4D active shape-changing architectures successfully, the rheological properties of the ink must be investigated first. Ink with low solid content shows low viscosity. It can easily be extruded from a micronozzle. However, the printed filament requires a lot of time to complete the liquid−solid transition because of the large amount of solvent. For ink with a higher solid content, the time for the liquid−solid transition greatly shortens, while the increased viscosity demands high pressure for extrusion. According to a previous study[40] and our own experiments, we summarized that c-PLA ink with a BP/PLA/DCM weight ratio of 0.1:1:3 and c-PLA/$Fe_3O_4$ ink with a $Fe_3O_4$/BP/PLA/DCM weight ratio of 0.25:0.1:1:3 presented satisfied rheological and printing capabilities. The process-related viscosity was discussed by capillary flow analysis inside the nozzle. Figure 1e shows the process-related viscosity of ink as a function of the process-related shear rate. c-PLA/$Fe_3O_4$ ink presented higher process-related viscosity than c-PLA ink because of the introduction of $Fe_3O_4$ nanoparticles, which indicated that c-PLA/$Fe_3O_4$ filaments were stiffer than c-PLA ones after extrusion.[24] Moreover, both c-PLA and c-PLA/$Fe_3O_4$


DOI: 10.1021/acsami.6b12824
ACS Appl. Mater. Interfaces 2017, 9, 876−883

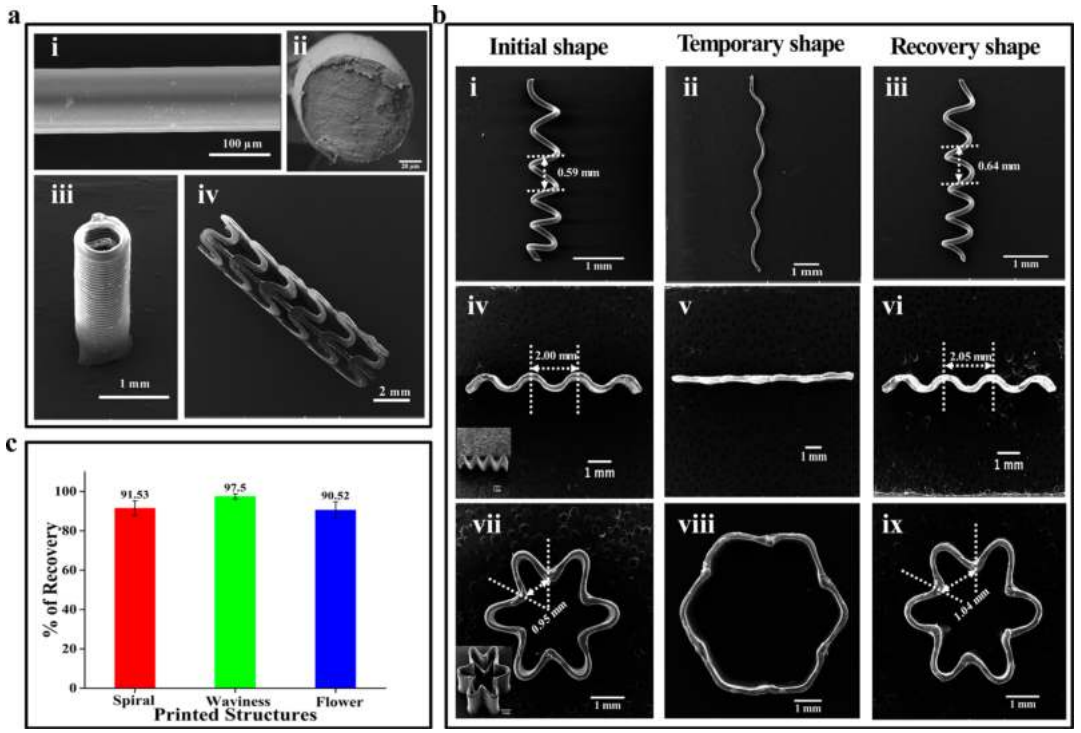


**Figure 2.** SEM images and 4D active shape-changing behavior of structures printed by c-PLA ink: (a) representative printed 4D active shape-changing architectures; (b) shape-changing behavior of select printed structures. (i–iii) The 3D microspiral is capable of memorizing a 1D linelike shape and then could recover to the original 3D microspiral upon application of heat stimuli. (iv–vi) The printed waviness-like shape could transfer from the temporary 2D sheet shape to the original 3D waviness shape under heat stimuli. (vii–ix) The flowerlike 3D configuration could be deformed to the temporary 3D hexagonal shape and could change to the initial 3D flowerlike configuration again upon exposure to heat stimuli. (c) Quantitative analysis of the shape-changing behavior of the select structures. Shape deformation and recovery of the 3D microspiral, 3D waviness-like structure, and 3D flowerlike structure happened in hot water with the temperature around 80 °C.

inks exhibited a shear-thinning performance because the process-related viscosity showed a declining trend as the process-related shear rate increased. Such capability guaranteed extrusion of inks from the micronozzle under high shear rates.

The solvent evaporation rate plays a key role in the fixation of printed structures after ink extrusion. To quantitatively investigate the evaporation behavior of DCM, the mass change of a filament was monitored once the filament was forced out from the nozzle. Figure 1f exhibits the DCM content of a 5 mm filament extruding from a nozzle with a 510 $\mu$m inner diameter changed with time. The initial DCM contents of c-PLA and c-PLA/$Fe_3O_4$ inks were lower than the preset fraction. This was caused by the fast evaporation of DCM during the original deposition process and the abrupt pressure drop taking place near the extruded point.[50] In the whole testing process, the real-time DCM content of c-PLA/$Fe_3O_4$ ink was less than that of c-PLA ink. This was contributed by the addition of $Fe_3O_4$ nanoparticles, which led to a more concentrated ink. Most DCM evaporated during the first 5 min (nearly 40–50%) for both c-PLA and c-PLA/$Fe_3O_4$ inks. Such fast evaporation behavior was a necessary condition for free DW printing in the open air. In our printing experiment, we chose the nozzle with 100 $\mu$m inner diameter, because DCM in the filament with a smaller diameter could take less time to diffuse from inside to the surface. This meant that a much faster solvent evaporation rate could be obtained and the rigidity of the printed structures could increase more rapidly. It is necessary to discuss the diameter shrinkage ratio ($D_s$) caused by DCM evaporation so that the geometrical changes can be evaluated. Figure S1 in the Supporting Information reveals that $D_s$ of the c-PLA/$Fe_3O_4$ filament was smaller than that of the c-PLA filament deposited by the nozzle with the same size and pressure. The underlying reason was the introduction of $Fe_3O_4$, causing a large solid content in c-PLA/$Fe_3O_4$ ink. Further, the $D_s$ values of both c-PLA and c-PLA/$Fe_3O_4$ were very small (lower than 3%), indicating that DCM evaporation had no apparent effect on the dimensions of the printed structures. This is important for constructing structures in precise sizes and geometries.

The macroscopic capabilities of the printed objects were discussed after the successful preparation of filaments. Gel fractions increased from 0% for PLA to 34.2% and 25.8% for c-PLA and c-PLA/$Fe_3O_4$, respectively (Figure S2 in the Supporting Information). This suggested the formation of cross-linking structures in the network. The lower gel fraction of c-PLA/$Fe_3O_4$ than c-PLA was due to the introduction of $Fe_3O_4$ nanoparticles that reduced the effective absorption of UV irradition.[34] c-PLA and c-PLA/$Fe_3O_4$ possessed a higher cold crystallization temperature ($T_{cc}$) and lower glass transition temperature ($T_g$), melting temperature ($T_m$), and crystallinity ($\chi_c$) in comparison PLA (Figure S3 and Table S1 in the Supporting Information). Such changes were caused by the formation of cross-linking networks and the negative influences of $Fe_3O_4$ nanoparticles on the development of crystallization in molecular structures.[34,48] Tensial tests (Figure S4 and Table S2 in the Supporting Information) revealed that the Young's modulus and maximum stress of the filaments after cross-linking decreased slightly. This was attributed to the dominent nature of the crystallinity for these parameters. However, the introduction of cross-links induced a decrease in the elongation at break and an increase in the stress at break. This suggested


DOI: 10.1021/acsami.6b12824
ACS Appl. Mater. Interfaces 2017, 9, 876–883

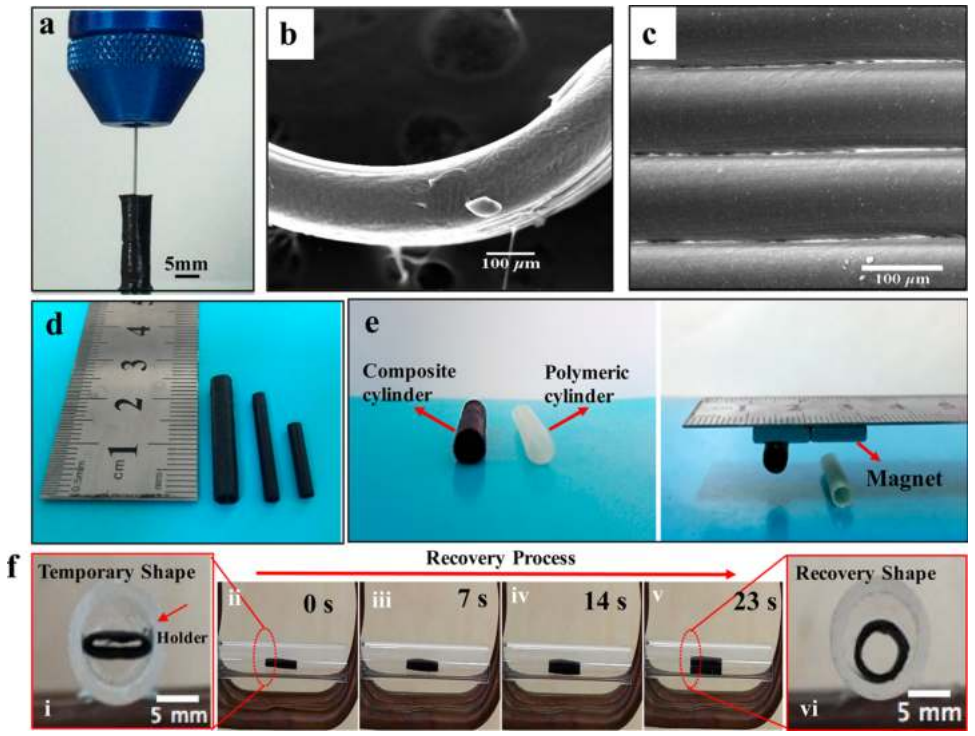


**Figure 3.** DW printing of 4D active shape-changing architectures by c-PLA/$Fe_3O_4$ ink: (a) optical image of the c-PLA/$Fe_3O_4$ composite ink depositing from a 150 $\mu$m micronozzle to create a self-supported multilayer composite tubular structure with 5 mm diameter; (b) SEM top view of the printed multilayer composite tubular structure; (c) SEM side view of the printed multilayer composite tubular structure; (d) printed composite cylinders with various sizes; (e) illustration of the responsive behavior of the composite cylinder under a constant magnetic field; (f) demonstration of the remote-actuated 4D shape-changing performance of a nanocomposite cylinder in a 30 kHz alternating magnetic field.

that the final mechanical propeties were sensitive to cross-linking.[51] A comparison between c-PLA and c-PLA/$Fe_3O_4$ revealed that $Fe_3O_4$ nanoparticles provided further reinforcement for the c-PLA polymer. The storage modulus at low temperature presented a changing trend similar to that of the tensial test, while above $T_g$, PLA presented the lowest storage modulus of the three samples. This was caused by the appearance of cross-linking structures in c-PLA and c-PLA/$Fe_3O_4$ (Figure S5a in the Supporting Information).[52] The $T_g$ values of PLA, c-PLA, and c-PLA/$Fe_3O_4$ are 74.5, 66.0, and 71.0 °C, respectively (Figure S5b in the Supporting Information), which were indispensable parameters for the shape memory performance. Shape memory cycles (SMCs) proceeding under controlled force mode were utilized to quantitatively characterize the shape memory behavior. To avoid the influence of stress history, a second SMC was used for analysis. Clearly, PLA, c-PLA, and c-PLA/$Fe_3O_4$ all presented excellent shape fixed behavior with a shape fixed ratio ($R_f$) above 90%. However, the shape recovery ratio ($R_r$) increased from 91.42% for PLA to 99.02% and 95.14% for c-PLA and c-PLA/$Fe_3O_4$, respectively (Figure S6 in the Supporting Information). The increase in $R_f$ was due to the irreversible slippages between molecules at temperatures above $T_g$ reduced by formation of the cross-linking network.[45,53] Such results demonstrated the effectiveness of improving the shape recovery behavior of PLA by the introduction of a UV cross-linking agent.

Various classes of 3D geometries with potential active shape-changing behavior were successfully constructed by c-PLA ink first through accurate control of the pressure and robot velocity. Scanning electron microscopy (SEM) images in Figure 2 show a group of 3D structures printed using a nozzle of 100 $\mu$m inner diameter. The straight fiber was deposited under a pressure of 1.4 MPa. The surface of the fiber was smooth, and its cross section was nearly round in shape [Figure 2a(i,ii)]. The microcylinder with 5 mm length and 400 $\mu$m radius was prepared under a pressure of 1.4 MPa and a velocity of 0.5 mm/s [Figure 2a(iii)]. A circular stent was constructed under the conditions of 1.75 MPa applied pressure and 0.4 mm/s velocity with a length of 12.8 mm and a diameter of 2.4 mm [Figure 2a(iv)]. Further interesting structures, including the freestanding 3D microspiral (an applied pressure of 1.75 MPa and a velocity of 0.4 mm/s) and a complex 3D waviness-like and flowerlike structure (an applied pressure of 1.4 MPa and a velocity of 0.5 mm/s), were printed to demonstrate the active shape-changing process (Figure 2b). At room temperature, these structures were in the glassy state. Once the temperature was higher than $T_g$ of the material, the structures turned rubbery and became flexible. In that case, they could be deformed to any shapes, which were able to be subsequently fixed by cooling below $T_g$. When reheated to a temperature above $T_g$, the deformed structures could return to their original printed shapes automatically. Figure 2b presents the shape-changing processes of selected structures, which qualitatively demonstrate that the configurations of printed architectures were capable of achieving 3D−1D−3D, 3D−2D−3D, and 3D−3D−3D transformations. The results indicate that a deformation dimension was presented, which was the key point of 4D.[26,54] The average dimensions of every repeat unit for both the initial and recovery structures are marked in Figure 2b to quantitatively analyze the shape-changing behavior of the printed geometries. According to eq 1, it can be determined that % $R$ of all of the structures printed by c-PLA ink were higher than 90% (Figure 2c). Especially for the waviness-like


DOI: 10.1021/acsami.6b12824
ACS Appl. Mater. Interfaces 2017, 9, 876−883

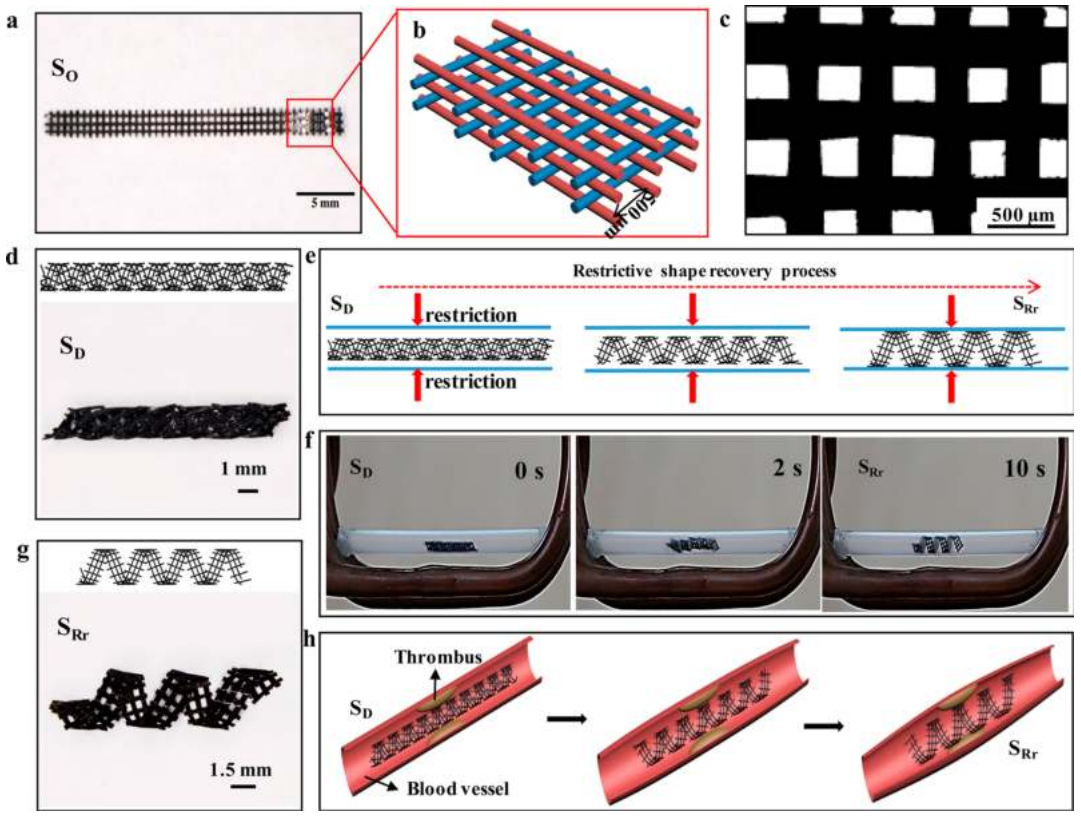


**Figure 4.** DW printing of a 4D scaffold by c-PLA/$Fe_3O_4$ ink and its potential biomedical application: (a) optical image of the multilayer scaffold; (b) schematic diagram of the detailed structure of the scaffold; (c) top view of the optical image of the printed scaffold; (d) deformation shape of the printed scaffold; (e) schematic of the restrictive shape recovery process; (f) demonstration of the restrictive shape recovery process triggered by a 30 kHz alternating magnetic field; (g) recovery shape under restrictive conditions; (h) potential application of the 4D scaffold as an intravascular stent. Here, the deformation temperature was 80 °C. $S_O$, $S_D$, and $S_{Rr}$ represent for the original, deformed, and recovery shapes under restrictive conditions, respectively.

structure, the one printed by c-PLA ink showed % $R$ = 97.5%, while that printed by PLA ink can only recover 86% of the original designed shape (Figures 2c and S6 in the Supporting Information). Obviously, the combination of UV cross-linking PLA shape memory materials with a DW printing method is an efficient and facile way to achieve 4D structures with satisfied shape-changing behavior.

After successfully fabricating 4D active shape-changing SMP-based architecture, we further investigated the printing of SMNC-based 4D active shape-changing architecture with functional behavior. In Figure 3a and movie S1 in the Supporting Information, it is seen that c-PLA/$Fe_3O_4$ composite ink could be printed into a 3D self-supported tubular structure (250 layers) with 5 mm diameter through a nozzle with 150 $\mu$m inner diameter. The SEM image in Figure 3b reveals that each layer of the printed structures was deposited precisely. Figure 3c demonstrates that interfaces between every adjacent layer were well connected with one another. By a suitable adjustment of the printing parameters, tubular structures with different custom-defined sizes could be obtained (Figure 3d). Parts e and f of Figure 3 exhibit the functionalities of 3D-printed nanocomposite structures. First, $Fe_3O_4$ nanoparticles endowed magnetism to the 3D-printed structures. In Figure 3e, the nanocomposite cylinder was able to be attracted by a magnet, indicating that the movement of the cylinder could be magnetically controlled and guided. Moreover, $Fe_3O_4$ nanoparticles were able to be used as internal heating sources in the presence of an alternating magnetic field. In Figure 3f, a 1-cm-long cylinder with 5 mm diameter was cut from the printed 2.5-cm-long tubule. It was then manually pressed into a flat shape at 80 °C and fixed by cooling to room temperature with an external force. Figure 3f(i) shows the cross section of the obtained temporary shape, which nearly became a linelike shape after pressing. Such a deformed shape was put into a 30 kHz alternating magnetic field together with a holder. The inside $Fe_3O_4$ nanoparticles could generate heat, causing the temporary shape to actively recover its initial configuration. Parts ii–v of Figure 3f present a set of side view images of the shape recovery process that completed in 23 s (movie S2 in the Supporting Information). When the recovery shape is checked, it can be found that the cross section went back to the circular shape [Figure 3f(vi)]. As a consequence, we achieved DW fabrication of SMNC-based 4D active shape-changing structures with magnetically guidable and remotely actuated performances.

Such a 4D active shape-changing structure has brilliant prospects to be applied in minimally invasive medical areas. Here, we demonstrated the potential application in self-expendable stents. We first printed a multilayer scaffold with a length of 30 mm and a width of 2 mm ($S_O$: original shape) using a nozzle of 150 $\mu$m inner diameter under a pressure of 1.4 MPa and a velocity of 2 mm/s (Figure 4a). Figure 4b provides the detailed structure of the scaffold, which was composed of five layers, and the interfilament space was 500 $\mu$m. The magnifying top view of the printed scaffold shows a 1D rectangular gridlike pattern (Figure 4c), which indicates the


DOI: 10.1021/acsami.6b12824
ACS Appl. Mater. Interfaces 2017, 9, 876–883

stable and accurate depositing behavior of the DW assembly. In Figure 4d, we deformed the scaffold to a spiral structure with 1 mm inner diameter ($S_D$: deformed shape). The schematic diagram in Figure 4e presents a restrictive shape memory process of our designed spiral structure. We assumed that the recovery shape could still be a spiral structure but with larger diameter ($S_{Rr}$: recovery shape under restrictive conditions) when the shape recovery process was triggered in a restrictive circumstance. Then, the self-expandable function could be achieved. To demonstrate the design strategy, the spiral structure with 1 mm inner diameter was put into a plastic tubular holder with 3 mm inner diameter. After they were placed together in a coil with an alternating magnetic field, the remotely actuated self-expandable behavior was monitored. The inner diameter of the spiral structure changed from 1 to 2.7 mm within 10 s (Figure 4f,g and movie S3 in the Supporting Information). Such a 4D scaffold exhibits great potential to be used as a self-expandable intravascular stent (Figure 4h). The diameter of the narrow vessel caused by thrombus could be reexpanded by applying the designed self-expandable stent to keep blood flowing normally. The addition of $Fe_3O_4$ nanoparticles offers such structure magnetically guided and remotely actuated behavior, which makes it much smarter and more convenient to be manipulated in body. A DW printing approach provides design freedom for the self-expendable stent, which is meaningful for the further development of user-defined intravascular stents and biomedical areas.

## CONCLUSIONS

In summary, we describe a powerful, general, and highly flexible approach to construct 4D active shape-changing structures by DW printing of UV cross-linking PLA-based inks. This technology represents an important strategy for the development of SMP-based materials. First, it enables unique and complex 4D active shape-changing architectures in either macro- or microscale with various geometries. Moreover, the technique realizes 4D printing of both SMPs and SMNCs and prepared 4D active shape-changing structures with remotely actuated and magnetically guidable behaviors that have great potential to be applied in minimally invasive medical areas. Although we focus on UV cross-linking PLA-based inks, such a technique could be extended to various functional inks for the design of 4D shape-changing structures with multifunctional capabilities based on its open design characteristics. This research has the potential to pave a new way for the further development of 4D printing, soft robotics, microsystems, and biomedical devices and beyond.

## MATERIALS AND METHODS

**Materials.** Semicrystalline thermoplastic PLA pellets (4032D) were purchased from Natureworks LLC. The weight-average molecular weight ($M_w$) of PLA pellets, tested by gel permeation chromatography, was 167 kDa. Benzophenone (BP) with 99% purity was supplied by Sigma-Aldrich. Dichloromethane (DCM) of analytical grade and $Fe_3O_4$ nanoparticles with 30 nm average diameter were commercially available from Aladdin Industrial Inc. To remove the influence of moisture, PLA pellets were dried at 50 °C for 24 h in a vacuum oven before use.

**Printing Ink Preparation.** The 25 wt % PLA polymeric ink was prepared by directly dissolving neat PLA pellets in DCM with a PLA/DCM weight ratio of 1:3. For 25 wt % c-PLA ink, BP was first dissolved in DCM with a weight ratio of 0.1:3. Then, neat PLA pellets were added to the above blend with a BP/PLA/DCM weight ratio of 0.1:1:3 for thorough mixing. A 25 wt % c-PLA/$Fe_3O_4$ composite ink was prepared by dissolving $Fe_3O_4$, BP, and PLA in DCM with a weight ratio of 0.25:0.1:1:9 through mechanical stirring in a sealed container. Then, the container with the above mixture was placed in an ultrasonic bath and kept open for DCM evaporation until the weight ratio of PLA/DCM was 1:3. All of the fabricating processes proceeded in light-resistant conditions at room temperature (25 ± 2 °C). The obtained ink was preserved in a sealed container until processing.

**Ink Characterization.** The process-related apparent viscosity of the prepared polymer ink was evaluated by a reported method based on capillary viscometry.[55] The ink was extruded from the nozzle with 200 μm inner diameter under UV irradiation. It was deposited onto a glass substrate for 60 s at a velocity of 1 mm/s under 10 different applied pressures (0.35−3.5 MPa) until extrusion of the ink achieved stable status. The obtained lines were dried at 50 °C for 12 h and then weighed by a high-precision electronic balance. The obtained masses, combined with the densities of the respective inks, were used to calculate the ink volumetric flow rate. Herein, equations including the Rabinowitsch correction were performed to determine the capillary data. Because the ratio of the length of the nozzle to its diameter exceeded 50, the end effects could be neglected.[55]

**Solvent Evaporation Rate Characterization.** The evaporation capability of DCM was investigated according to a previous study.[56] The ink was extruded from a 510-μm-diameter nozzle under a pressure of 420 kPa. A 5 mm filament was deposited onto a glass substrate placed on a high-precision electronic balance. The weight of the filament was monitored for 6 h and recorded as a real-time mass. Then, the filament was dried in a 50 °C vacuum oven for 12 h. After that, the above filament was weighed again to obtain the dried mass. The real-time solvent percentage was used to evaluate the solvent evaporation capabilities.

**Diameter Shrinkage Ratio Characterization.** The ink was extruded out of the nozzle with 100 μm inner diameter at a pressure of 1.4 MPa under UV irradiation. The depositing filaments were collected and dried in a vacuum oven at 50 °C for 12 h. The obtained filaments were cut into 10-mm-long sections for each composition. Then, an optical microscope (Olympus SZX16) was used to measure the actual diameter of the filaments. The diameter shrinkage ratio ($D_s$) was calculated as follows:

$$D_s = (D_n - D_a)/D_n \times 100\% \quad (1)$$

where $D_n$ is the inner diameter of the nozzle used and $D_a$ is the actual diameter of the corresponding filament after drying.

**DW Fabrication of a 4D Active Shape-Changing Architecture.** The DW printing of the ink was carried out by a system consisting of a microdepositing robot (I&J2200-4, I&J Fisnar) controlled by computer software (JR Points for Dispensing, Janome Sewing Machine), a dispensing apparatus (HP-7X, EFD), and two 365 nm UV LEDs with 450 mW/cm$^2$ intensity (UPUL012, Landun). The designed 3D structures could be constructed by accurate computer control of the applied pressure, moving velocity, and direction of the robot. The rapid evaporation of DCM in the printing process functioned to harden the 3D structures. The enhanced shape memory behavior could be obtained through UV irradiation. The filament was deposited under 1.4 MPa. The supported structures (cylinder, waviness, and flower) were fabricated under a pressure of 1.4 MPa and a robot velocity 0.5 mm/s. The spiral and stent were built under the conditions of 1.75 MPa pressure and 0.4 mm/s robot velocity.

**Shape-Changing Behavior Characterization.** The printed 3D architecture was heated to 80 °C (a temperature above $T_g$). After being soft, the heated structure was deformed to the desired configuration under an external force. The temporary architecture was fixed by cooling to room temperature. The heat-actuated active shape-changing processes were monitored by placing the deformed objects into hot water around 80 °C. To quantitatively investigate the shape-changing behavior of the printed 3D structures, the dimensions of every repeated unit for both the initial and recovery structures were measured to obtain the average dimensions of repeated units for every structure. % $R$ (percentage of shape recovery), using to characterize the recovery degree of the printed geometries, could be obtained as follows:


DOI: 10.1021/acsami.6b12824
ACS Appl. Mater. Interfaces 2017, 9, 876−883

$$\% R = (l_r - l_o)/l_o \times 100\% \quad (2)$$

where $l_o$ and $l_r$ represent the average dimensions of repeated units for the original and recovery structures, respectively. Remotely induced shape-changing processes were monitored by putting the deformed objects into an alternating magnetic field of 30 kHz. A scanning electron microscope (TESCAN VEGA3SB) and an optical microscope (Olympus SZX16) were used to observe the morphologies of the original, temporary, and recovery structures during the shape-changing process.

## ■ ASSOCIATED CONTENT

### Supporting Information

The Supporting Information is available free of charge on the ACS Publications website at DOI: 10.1021/acsami.6b12824.

Full experimental details, including characterization of the described materials, additional data, figures, tables, and movies (PDF)

3D printing process of the composite cylinder (MOV)

Shape recovery process of the printed composite cylinder triggered by a 30 kHz alternating magnetic field (MOV)

Self-expandable behavior of the spiral stent actuated by a 30 kHz alternating magnetic field (MOV)

## ■ AUTHOR INFORMATION


### Corresponding Author

*E-mail: lengjs@hit.edu.cn (J.L.).

### ORCID

Jinsong Leng: 0000-0001-5098-9871


### Author Contributions

H.W., Q.Z., Y.L., L.L., and J.L. conceived the research. H.W. and Q.Z. performed the experiments and analyzed the experimental results. H.W. composed the manuscript. Y.Y., L.L., and Y.L. offered advice on grammar revisions. J.L. oversaw the preparation of the manuscript. All authors reviewed the manuscript.

### Notes

The authors declare no competing financial interest.

## ■ ACKNOWLEDGMENTS

This work was supported by the National Natural Science Foundation of China (Grant 11225211), for which we are very grateful.

## ■ REFERENCES


(1) Yu, K.; Ge, Q.; Qi, H. J. Reduced Time as a Unified Parameter Determining Fixity and Free Recovery of Shape Memory Polymers. *Nat. Commun.* **2014**, *5*, 3066.

(2) Meng, H.; Li, G. Q. A Review of Stimuli-responsive Shape Memory Polymer Composites. *Polymer* **2013**, *54* (9), 2199–2221.

(3) Hu, J. L.; Zhu, Y.; Huang, H. H.; Lu, J. Recent Advances in Shape-memory Polymers: Structure, Mechanism, Functionality, Modeling and Applications. *Prog. Polym. Sci.* **2012**, *37* (12), 1720–1763.

(4) Leng, J. S.; Lan, X.; Liu, Y. J.; Du, S. Y. Shape-memory Polymers and Their Composites: Stimulus Methods and Applications. *Prog. Mater. Sci.* **2011**, *56* (7), 1077–1135.

(5) Grubbs, R. B.; Sun, Z. Shape-changing Polymer Assemblies. *Chem. Soc. Rev.* **2013**, *42* (17), 7436–7445.

(6) Erb, R. M.; Sander, J. S.; Grisch, R.; Studart, A. R. Self-shaping Composites with Programmable Bioinspired Microstructures. *Nat. Commun.* **2013**, *4*, 1712.

(7) Zhao, Q.; Qi, H. J.; Xie, T. Recent Progress in Shape Memory Polymer: New Behavior, Enabling Materials, and Mechanistic Understanding. *Prog. Polym. Sci.* **2015**, *49–50*, 79–120.

(8) Liu, Y. J.; Du, H. Y.; Liu, L. W.; Leng, J. S. Shape Memory Polymers and Their Composites in Aerospace Applications: A Review. *Smart Mater. Struct.* **2014**, *23* (2), 023001.

(9) Bao, M.; Lou, X. X.; Zhou, Q. H.; Dong, W.; Yuan, H. H.; Zhang, Y. Z. Electrospun Biomimetic Fibrous Scaffold from Shape Memory Polymer of PDLLA-co-TMC for Bone Tissue Engineering. *ACS Appl. Mater. Interfaces* **2014**, *6* (4), 2611–2621.

(10) Lendlein, A.; Langer, R. Biodegradable, Elastic Shape-memory Polymers for Potential Biomedical Applications. *Science* **2002**, *296* (5573), 1673–1676.

(11) Liu, X.; Zhao, K.; Gong, T.; Song, J.; Bao, C. Y.; Luo, E.; Weng, J.; Zhou, S. B. Delivery of Growth Factors Using a Smart Porous Nanocomposite Scaffold to Repair a Mandibular Bone Defect. *Biomacromolecules* **2014**, *15* (3), 1019–1030.

(12) Xie, M. H.; Wang, L.; Ge, J.; Guo, B. L.; Ma, P. X. Strong Electroactive Biodegradable Shape Memory Polymer Networks Based on Star-Shaped Polylactide and Aniline Trimer for Bone Tissue Engineering. *ACS Appl. Mater. Interfaces* **2015**, *7* (12), 6772–6781.

(13) Guo, B. C.; Chen, Y. W.; Lei, Y. D.; Zhang, L. Q.; Zhou, W. Y.; Rabie, A. B. M.; Zhao, J. Q. Biobased Poly(propylene sebacate) as Shape Memory Polymer with Tunable Switching Temperature for Potential Biomedical Applications. *Biomacromolecules* **2011**, *12* (4), 1312–1321.

(14) Hager, M. D.; Bode, S.; Weber, C.; Schubert, U. S. Shape Memory Polymers: Past, Present and Future Developments. *Prog. Polym. Sci.* **2015**, *49–50*, 3–33.

(15) Zarek, M.; Layani, M.; Cooperstein, I.; Sachyani, E.; Cohn, D.; Magdassi, S. 3D printing of shape memory polymers for flexible electronic devices. *Adv. Mater.* **2016**, *28* (22), 4449–4454.

(16) Zhou, Y.; Huang, W. M.; Kang, S. F.; Wu, X. L.; Lu, H. B.; Fu, J.; Cui, H. P. From 3D to 4D Printing: Approaches and Typical Applications. *J. Mech. Sci. Technol.* **2015**, *29* (10), 4281–4288.

(17) Kratz, K.; Voigt, U.; Lendlein, A. Temperature-memory Effect of Copolyesterurethanes and Their Application Potential in Minimally Invasive Medical Technologies. *Adv. Funct. Mater.* **2012**, *22* (14), 3057–3065.

(18) Yu, Z. B.; Zhang, Q. W.; Li, L.; Chen, Q.; Niu, X. F.; Liu, J.; Pei, Q. B. Highly Flexible Silver Nanowire Electrodes for Shape-memory Polymer Light-emitting Diodes. *Adv. Mater.* **2011**, *23* (5), 664–668.

(19) Stansbury, J. W.; Idacavage, M. J. 3D Printing with Polymers: Challenges among Expanding Options and Opportunities. *Dent. Mater.* **2016**, *32* (1), 54–64.

(20) Tumbleston, J. R.; Shirvanyants, D.; Ermoshkin, N.; Janusziewicz, R.; Johnson, A. R.; Kelly, D.; Chen, K.; Pinschmidt, R.; Rolland, J. P.; Ermoshkin, A.; Samulski, E. T.; DeSimone, J. M. Continuous Liquid Interface Production of 3D Objects. *Science* **2015**, *347* (6228), 1349–1352.

(21) Trimmer, B.; Lewis, J. A.; Shepherd, R. F.; Lipson, H. 3D Printing Soft Materials: What is Possible? *Soft Robot.* **2015**, *2* (1), 3–6.

(22) Lewis, J. A.; Ahn, B. Y. Three-dimensional Printed Electronics. *Nature* **2015**, *518* (7537), 42–43.

(23) Kokkinis, D.; Schaffner, M.; Studart, A. R. Multimaterial Magnetically Assisted 3D Printing of Composite Materials. *Nat. Commun.* **2015**, *6*, 8643.

(24) Guo, S. Z.; Yang, X. L.; Heuzey, M. C.; Therriault, D. 3D Printing of a Multifunctional Nanocomposite Helical Liquid Sensor. *Nanoscale* **2015**, *7* (15), 6451–6456.

(25) Pawar, A. A.; Saada, G.; Cooperstein, I.; Larush, L.; Jackman, J. A.; Tabaei, S. R.; Cho, N.-J.; Magdassi, S. High-performance 3D Printing of Hydrogels by Water-dispersible Photoinitiator Nanoparticles. *Sci. Adv.* **2016**, *2* (4), e1501381.

(26) Gladman, A. S.; Matsumoto, E. A.; Nuzzo, R. G.; Mahadevan, L.; Lewis, J. A. Biomimetic 4D Printing. *Nat. Mater.* **2016**, *15* (4), 413–418.




DOI: 10.1021/acsami.6b12824
*ACS Appl. Mater. Interfaces* 2017, 9, 876–883

(27) Sun, Y. J.; Soh, S. Printing Tablets with Fully Customizable Release Profiles for Personalized Medicine. *Adv. Mater.* **2015**, *27* (47), 7847−7853.
(28) Hinton, T. J.; Jallerat, Q.; Palchesko, R. N.; Park, J. H.; Grodzicki, M. S.; Shue, H.-J.; Ramadan, M. H.; Hudson, A. R.; Feinberg, A. W. Three-dimensional Printing of Complex Biological Structures by Freeform Reversible Embedding of Suspended Hydrogels. *Sci. Adv.* **2015**, *1* (9), e1500758.
(29) Yang, Y.; Chen, Y.; Wei, Y.; Li, Y. 3D Printing of Shape Memory Polymer for Functional Part Fabrication. *Int. J. Adv. Manuf. Technol.* **2016**, *84* (9), 2079−2095.
(30) Mao, Y. Q.; Yu, K.; Isakov, M. S.; Wu, J. T.; Dunn, M. L.; Qi, H. J. Sequential Self-folding Structures by 3D Printed Digital Shape Memory Polymers. *Sci. Rep.* **2015**, *5*, 13616.
(31) Ge, Q.; Qi, H. J.; Dunn, M. L. Active Materials by Four-dimension Printing. *Appl. Phys. Lett.* **2013**, *103* (13), 131901.
(32) Li, W. B.; Liu, Y. J.; Leng, J. S. Selectively Actuated Multi-shape Memory Effect of a Polymer Multicomposite. *J. Mater. Chem. A* **2015**, *3* (48), 24532−24539.
(33) Razzaq, M. Y.; Behl, M.; Kratz, K.; Lendlein, A. Multifunctional Hybrid Nanocomposites with Magnetically Controlled Reversible Shape-memory Effect. *Adv. Mater.* **2013**, *25* (40), 5730−5733.
(34) Gong, T.; Li, W. B.; Chen, H. M.; Wang, L.; Shao, S. J.; Zhou, S. B. Remotely Actuated Shape Memory Effect of Electrospun Composite Nanofibers. *Acta Biomater.* **2012**, *8* (3), 1248−1259.
(35) Kumar, U. N.; Kratz, K.; Heuchel, M.; Behl, M.; Lendlein, A. Shape-memory Nanocomposites with Magnetically Adjustable Apparent Switching Temperatures. *Adv. Mater.* **2011**, *23* (36), 4157−4162.
(36) Zheng, X. T.; Zhou, S. B.; Xiao, Y.; Yu, X. J.; Li, X. H.; Wu, P. Z. Shape Memory Effect of Poly(D,L-lactide)/Fe3O4 Nanocomposites by Inductive Heating of Magnetite Particles. *Colloids Surf., B* **2009**, *71* (1), 67−72.
(37) Yu, X. J.; Zhou, S. B.; Zheng, X. T.; Guo, T.; Xiao, Y.; Song, B. T. A Biodegradable Shape-memory Nanocomposite with Excellent Magnetism Sensitivity. *Nanotechnology* **2009**, *20* (23), 235702.
(38) Kolesky, D. B.; Truby, R. L.; Gladman, A. S.; Busbee, T. A.; Homan, K. A.; Lewis, J. A. 3D Bioprinting of Vascularized, Heterogeneous Cell-laden Tissue Constructs. *Adv. Mater.* **2014**, *26* (19), 3124−3130.
(39) Sun, K.; Wei, T. S.; Ahn, B. Y.; Seo, J. Y.; Dillon, S. J.; Lewis, J. A. 3D Printing of Interdigitated Li-Ion Microbattery Architectures. *Adv. Mater.* **2013**, *25* (33), 4539−4543.
(40) Guo, S. Z.; Gosselin, F.; Guerin, N.; Lanouette, A. M.; Heuzey, M. C.; Therriault, D. Solvent-cast Three-dimensional Printing of Multifunctional Microsystems. *Small* **2013**, *9* (24), 4118−4122.
(41) Hanson Shepherd, J. N.; Parker, S. T.; Shepherd, R. F.; Gillette, M. U.; Lewis, J. A.; Nuzzo, R. G. 3D Microperiodic Hydrogel Scaffolds for Robust Neuronal Cultures. *Adv. Funct. Mater.* **2011**, *21* (1), 47−54.
(42) Lebel, L. L.; Aissa, B.; El Khakani, M. A.; Therriault, D. Ultraviolet-assisted Direct-write Fabrication of Carbon Nanotube/Polymer Nanocomposite Microcoils. *Adv. Mater.* **2010**, *22* (5), 592−596.
(43) Lewis, J. A. Direct Ink Writing of 3D Functional Materials. *Adv. Funct. Mater.* **2006**, *16* (17), 2193−2204.
(44) Gratson, G. M.; Lewis, J. A. Phase Behavior and Rheological Properties of Polyelectrolyte Inks for Direct-write Assembly. *Langmuir* **2005**, *21* (1), 457−464.
(45) Yuan, D. S.; Chen, Z. H.; Xu, C. H.; Chen, K. L.; Chen, Y. K. Fully Biobased Shape Memory Material based on Novel Cocontinuous Structure in Poly(lactic acid)/Natural Rubber TPVs Fabricated via Peroxide-induced Dynamic Vulcanization and in situ Interfacial Compatibilization. *ACS Sustainable Chem. Eng.* **2015**, *3* (11), 2856−2865.
(46) Samuel, C.; Barrau, S.; Lefebvre, J. M.; Raquez, J. M.; Dubois, P. Designing Multiple-shape Memory Polymers with Miscible Polymer Blends: Evidence and Origins of a Triple-shape Memory Effect for Miscible PLLA/PMMA Blends. *Macromolecules* **2014**, *47* (19), 6791−6803.
(47) Yan, B. B.; Gu, S. Y.; Zhang, Y. H. Polylactide-based Thermoplastic Shape Memory Polymer Nanocomposites. *Eur. Polym. J.* **2013**, *49* (2), 366−378.
(48) Koo, G. H.; Jang, J. Preparation of Melting-free Poly(lactic acid) by Amorphous and Crystal Crosslinking under UV Irradiation. *J. Appl. Polym. Sci.* **2013**, *127* (6), 4515−4523.
(49) Decker, C. Photoinitiated Crosslinking Polymerisation. *Prog. Polym. Sci.* **1996**, *21* (4), 593−650.
(50) Bruneaux, J.; Therriault, D.; Heuzey, M. C. Micro-extrusion of Organic Inks for Direct-write Assembly. *J. Micromech. Microeng.* **2008**, *18* (11), 115020.
(51) Dolog, R.; Weiss, R. A. Shape Memory Behavior of a Polyethylene-Based Carboxylate Ionomer. *Macromolecules* **2013**, *46* (19), 7845−7852.
(52) Wang, Z. W.; Zhao, J.; Chen, M.; Yang, M. H.; Tang, L. Y.; Dang, Z. M.; Chen, F. H.; Huang, M. M.; Dong, X. Dually Actuated Triple Shape Memory Polymers of Cross-linked Polycyclooctene-carbon Nanotube/Polyethylene Nanocomposites. *ACS Appl. Mater. Interfaces* **2014**, *6* (22), 20051−20059.
(53) Jing, X.; Mi, H. Y.; Peng, X. F.; Turng, L. S. The Morphology, Properties, and Shape Memory Behavior of Polylactic Acid/Thermoplastic Polyurethane Blends. *Polym. Eng. Sci.* **2015**, *55* (1), 70−80.
(54) Tibbits, S. 4D Printing: Multi-material Shape Change. *Archit. Des.* **2014**, *84* (1), 116−121.
(55) Chai, Z. H.; Shi, B. C.; Guo, Z. L.; Rong, F. M. Multiple-relaxation-time Lattice Boltzmann Model for Generalized Newtonian Fluid Flows. *J. Non-Newtonian Fluid Mech.* **2011**, *166* (5−6), 332−342.
(56) Guo, S. Z.; Heuzey, M. C.; Therriault, D. Properties of Polylactide Inks for Solvent-cast Printing of Three-dimensional Freeform Microstructures. *Langmuir* **2014**, *30* (4), 1142−1150.


DOI: 10.1021/acsami.6b12824
*ACS Appl. Mater. Interfaces* 2017, 9, 876−883